Heliyon 6 (2020) e04492

Contents lists available at ScienceDirect

Heliyon

journal homepage: www.cell.com/heliyon

Research article

Improved phenol sequestration from aqueous solution using silver nanoparticle modified Palm Kernel Shell Activated Carbon

M.O. Aremu [a], A.O. Arinkoola [a,b,*], I.A. Olowonyo [a], K.K. Salam [a]

[a] Department of Chemical Engineering, Ladoke Akintola University of Technology, Ogbomoso, Nigeria
[b] Department of Petroleum Engineering, African University of Science and Technology (AUST), Abuja, Nigeria

ARTICLE INFO

Keywords:
Chemical engineering
Environmental science
Nanotechnology
Materials application
Materials characterization
Materials processing
Materials synthesis
Thermal synthesis
Production optimization
Isotherms
Kinetics
Percentage removal

ABSTRACT

Modified Palm Kernel Shell Activated Carbon (PKSAC) using silver nanoparticle (Ag-NPs-PKSAC) was investigated on phenol uptake from aqueous solution. Effects of temperature (500–700 °C), time (90–120 min), and alkaline concentration (0.1–0.5 M) were studied on the yield and methylene blue numbers for the synthesis. Effects of initial concentration (100–200 mg/L), agitation (150–250 rpm), contact time (30–120 min), and adsorbent dosage (0.15–0.25 g) were studied in a batch experiment on percentage removal of phenol. The PKS, char, PKSAC and Ag-NPs-PKSAC were characterized using BET, FTIR, SEM, and proximate analyses. The synthesis of PKSAC was optimum at 608 °C, 0.5 M KOH, and carbonization holding time of 60 min. The optimum phenol uptake was 85.64, 90.29 and 91.70% for PKSAC, Ag-NPs-PKSAC, and commercial adsorbent, respectively. The adsorption mechanism of phenol followed the Langmuir isotherm and best described as physio-sorption with pseudo-second-order kinetics. Phenol exhibits high affinity (ΔS° = 0.0079 kJ/mol K) for Ag-NPs-PKSAC with favorable adsorption (ΔG° = -1.551 kJ/mol) at high temperature due to endothermic (ΔH° = 1.072 kJ/mol) nature of the system. The result obtained in this study compared favorably with the literature.

1. Introduction

Industrial effluents represent important and major sources through which substantial organic and inorganic wastes find their ways into the water bodies. The consequent accumulation of these wastes in water bodies, constitute a serious environmental hazard to human, plants, and animals (Fuf and Wang, 2011). Wastewater may contain a wide variety of chemicals such as organic salts, aliphatic and aromatic hydrocarbons, oils and greases, metals, and occasionally radioactive materials (Cerqueira and Costa Marques, 2012). One of the most hazardous pollutants present in industrial wastewater discharge is phenol. It is toxic, highly combustible, and soluble in water, oils, carbon disulfide as well as in numerous other organic solvents (AbdelWahab et al., 2009). Because of its solubility in natural water, the formation of other toxic substituted compounds has been reported (Busca et al., 2008).

Many techniques such as microbial degradation, chemical oxidation, enzymatic polymerization, membrane separation, solvent extraction, photocatalytic degradation, and adsorption have been applied to remove phenol from wastewater (Shourian et al., 2009; Wang et al., 2018; Busca et al., 2008; El-Nas et al., 2009). Adsorption techniques using activated carbon had proven to be a very effective method for environmental control and wastewater management (Okeowo et al., 2020). Conventional techniques are limited due to relatively low efficiency especially where micropollutants are involved. The high polarity and/or chemical persistence of phenolic compounds and other micro-organic pollutants make them escape from the conventional wastewater treatment plants and only about 21–40%removal efficiency has been reported (Murniati et al., 2017). Adsorption method is preferable, because of its flexibility, better efficiency compared to other methods, and relatively cheap (Zhang et al., 2017). For commercial feasibility, efforts have been directed to developing low-cost adsorbents by using agricultural residues. Several agricultural residues such as fruits, rice husk, straw, coconut wastes, coffee waste, vegetable peels bagasse, etc had been investigated in this regard (Balakrishnan and Batra, 2011; Bhatnagar et al., 2011, 2015; Devi and Saroha, 2016; Hafshejani et al., 2016).

Specifically, the application of agricultural waste adsorbent for the removal of different organic pollutants from wastewater and soil has produced remarkable results. For example, the agricultural waste adsorbent was successfully deployed for the removal of different varieties of dyes (Chebli et al., 2015; Nayak and Pal, 2017; Wang et al., 2017). Portinho et al. (2017), utilized activated carbon produced from grape stalk to remove caffeine drugs from wastewater. Another drug, tylosin,

* Corresponding author.
E-mail addresses: aoarinkoola@lautech.edu.ng, moranroolaakeem@yahoo.com (A.O. Arinkoola).

https://doi.org/10.1016/j.heliyon.2020.e04492
Received 19 May 2020; Received in revised form 4 July 2020; Accepted 14 July 2020

was removed from an aqueous solution using goethite modified adsorbent produced from the straw mass (Yin et al., 2016). Other organic pollutants that have been resolved using agricultural waste adsorbents include, pesticides (metalaxyl, metribuzin, 2,4-dichlorophenoxyacetic acid) (Gamiz et al., 2016; Peña et al., 2016; Trivedi et al., 2016) and aromatic compounds (polycyclic aromatic hydrocarbons, phenol) (Karri et al., 2017). In all aforementioned studies, developing the properties of green adsorbents to merge the commercial ones in terms of adsorptive capacities remains a challenge. To improve the performance of AC derived from various materials, chemical or physical activation is often performed. In the physical activation, the feedstock is carbonized to its char at a predetermined temperature to eliminate volatile components and the char further heated under purified nitrogen before activated under CO_2 at specific temperature and time to produce the desired activated carbon (Bello et al., 2019). On the other hand, in chemical activation, the feedstock is impregnated with acid or alkali for a specific time followed by carbonization or vice versa (Okeowo et al., 2020). Chemical treatments have been applied to improve the surface area, pore size distribution, and functional groups present on the surface of an adsorbent for enhanced adsorption capacity of activated carbon (Wan Ngah and Hanafiah, 2008; Cheung et al., 2012). For example, the acid treatment causes high acidity, relatively low surface areas, and pore volumes. The reduction of porosity may affect adsorption capacity.

In this study, the effect of silver nanoparticles impregnation into alkali-treated Palm Kernel Shell Activated Carbon (PKSAC) was investigated for the removal of phenol in simulated wastewater. We integrated nanotechnology, experimental design, response surface methodology, and quantitative solution in a single framework to optimize the yield and improve the physicochemical properties of AC from PKS. The biotechnology adopted using plant extract is sustainable, cheap, simple, environment friendly, and reproducible. The MBN and yield criteria for optimization during the AC development offer a quick alternative characterization approach to sophisticated analytical equipment.

2. Materials and equipment

The PKS was obtained from a local palm oil industry at Aroje, Ogbomoso, Oyo State, Nigeria. The reagents used for the study include KOH, $AgNO_3$, distilled water, HCl, Phenol (Sigma Aldrich, 99.9% purity), Methylene Blue ($C_{16}H_{18}ClN_3S{\cdot}xH_2O$, 99.1% by HPLC). The equipment used include weighing balance (ZC20602), UV-vis (UV752(D), FTIR, SEM (JSM-7600F)), Crusher, Stop Watch, Desiccators, Water Bath Shaker, rotary shaker (HZ 300), muffle furnace (Carbolite ELF 11/68) and Electric Oven (Techmel TT-9083, USA).

2.1. Silver nanoparticles

The silver nanoparticle (Ag-NPs) used for our investigation was procured from the Microbiology Laboratory, Ladoke Akintola University of Technology, Ogbomoso. The precursor for simple step synthesis was $AgNO_3$ while extracts from the shell of Cola nitida served as a capping agent. The extracts from the shell of Cola nitida fruit were obtained by suspending 1 g of milled pod in 100 ml of distilled water and heated in a water bath at a temperature of 60 °C for 1 h and filtered to obtain the extract. To synthesize the nanoparticles, 10 ml of the extract was added to 40 ml (1mM) $AgNO_3$ solution in a reaction vessel for the reduction of silver ion to silver nanoparticles. The reaction was carried out at room temperature for 2 h at 100 rpm. The formation of silver nanoparticles was monitored through a change of colour observed as reaction proceeds. At the end of the reaction, the solution absorbance was analyzed using UV-Vis spectroscopy. Further characterization was done using Transmission Electron Microscopy (TEM) and Fourier-Transform Infrared (FTIR) Analyses to study the shape and size and dominant functional groups. The particles were spherical in shape and poly-disperse in nature, with sizes ranging from 12 to 80 nm. The production and characterization of the nanoparticles are available in Lateef et al. (2016).

2.2. Synthesis of activated carbon from Palm Kernel Shell

The PKS was washed with water and dried at 110 °C for 24 h to remove moisture. A portion of the dried PKS was pulverized then ground to powder and sieved to a particle size of 1–2 mm. 20 g of the sample was then mixed by impregnation in KOH (0.1–0.5 mg/L) based on the impregnation ratio of 1. The KOH soaked samples were kept for 24 h in a furnace at ambient conditions. Excess KOH was drained and evaporated between 100-105 °C for 4 h. The slurry PKS was activated in a muffle at varied temperatures (500–700 °C) and time (90–120 min). To optimize process variables, the experiment was designed using the Box-Behnken algorithm (Table 1). The selection of optimum conditions was done numerically using desirability objective function embedded in Design-Expert version 11. Methylene Blue Number (MBN) and product yield are the responses estimated using Eqs. (1) and (2). The activated char was neutralized using deionized water until the pH of the washing solution was in the range of 6.5–7.0. The neutralized char was dried in the oven between 80 - 90 °C for 2 h and granular activated carbon termed PKSAC was obtained. The PKSAC at optimum condition was characterized.

$$MBN\left(\frac{mg}{g}\right) = \left(\frac{C_o - C_e}{M}\right) \times V \tag{1}$$

$$Yield(\%) = \frac{w_c}{w_o} \times 100 \tag{2}$$

2.3. Impregnation of PKSAC with Ag-NPs

5 g of PKSAC was dispersed in 100 ml of Ag-NPs solution (0.17 mg/L) contained in a 250 ml Erlenmeyer flask. The mixture was agitated with magnetic stirring at ambient temperature for 12 h to ensure homogenous slurry of the mixture. After the mixing period, the product Ag-NPs–PKSAC was oven-dried at 110 °C for 10 h.

2.4. Products characterization

Fourier transform infrared (FTIR) spectroscope (FTIR-2000, Perkin Elmer) was used to study the characteristic functional groups on the surface of the products. The spectra were measured from 500 to 4000 cm^{-1}. A scanning electron microscope (SEM-Jeol, JSM-7600F) was

Table 1. Box-Behnken matrix with yield and MBN.

Runs	Factors			Responses	
	A: Conc. (mg/L)	B: Temp. (°C)	C: Time (min)	Yield (%)	MBN (mg/g)
1	0.3	600	105	24.70	17.06
2	0.1	700	105	23.25	31.18
3	0.3	500	90	22.00	25.29
4	0.3	600	105	25.95	16.98
5	0.1	500	105	19.35	14.12
6	0.5	500	105	23.05	30.00
7	0.5	600	120	23.33	25.98
8	0.3	600	105	23.30	16.39
9	0.3	600	105	23.40	16.96
10	0.1	600	90	27.75	3.76
11	0.5	700	105	27.05	8.24
12	0.3	700	120	25.70	7.53
13	0.1	600	120	27.85	4.71
14	0.5	600	90	32.30	35.88
15	0.3	700	90	28.75	10.59
16	0.3	500	120	17.90	4.12
17	0.3	600	105	26.65	15.07

Table 2. Process variables and their levels.

Factors	Unit	Level	
		Low	High
Contact time	Min	60	150
Adsorbent Dosage	g	0.15	0.25
Initial concentration	Mg/L	50	200
Agitation rate	rpm	150	250

employed for examining the surface morphology of the products. The surface area, micropore volume, total pore volume of the adsorbents were analyzed using Brunauer–Emmett–Teller (BET). The proximate and ultimate analyses were obtained using a thermogravimetric analyzer (Perkin Elmer TGA7).

2.5. Adsorption experiment

Batch adsorption experiments were performed to determine the adsorption capacity of PKSAC and Ag-NPs-PKSAC in terms of percentage phenol removed from the solution. The residual phenol concentrations were determined after the withdrawal of the sample solution at equilibrium. To lessen the product fines interfering in the analysis, solutions were filtered prior to analysis. Equilibrium studies were performed for 5 h with a plot of absorbance versus phenol concentrations, a linear - Lambert relationship was established between absorbance and concentration. The concentrations of phenol solution before and after adsorption were quantified with UV-Vis spectrophotometer (UV – 752, USA) at a maximum wavelength of 296 nm. The percentage of phenol removed was estimated using Eq. (3).

$$\%\ Phenol\ removal = \frac{(C_o - C_e)}{C_o} \times 100 \quad (3)$$

Where, C_o and C_e (mg/L) are the liquid-phase phenol concentrations at initial and equilibrium, respectively.

To study simultaneously, the effect of initial concentration, contact time, agitation rate, and concentration of phenol on percentage removed, 100 ml of phenol solution with initial concentration ranged between 50 – 200 mg/l were prepared in a series of 200 ml Erlenmeyer flasks. Varied mass of adsorbents (0.1–0.25 g) was mixed with 25 ml of

Table 3. Analysis of variance for yield and MBN.

	MODEL	Sum of square	df	Mean square	F-value	p-value
Yield (%)	Quadratic	183.82	7	26.26	20.54	0.0002
				$R^2 = 0.954$	Adj. $R^2 = 0.901$	Pred. $R^2 = 0.876$
MBN (mgg^{-1})	Quadratic	147.63	9	23.07	23.07	0.001
				$R^2 = 0.977$	Adj. $R^2 = 0.934$	-

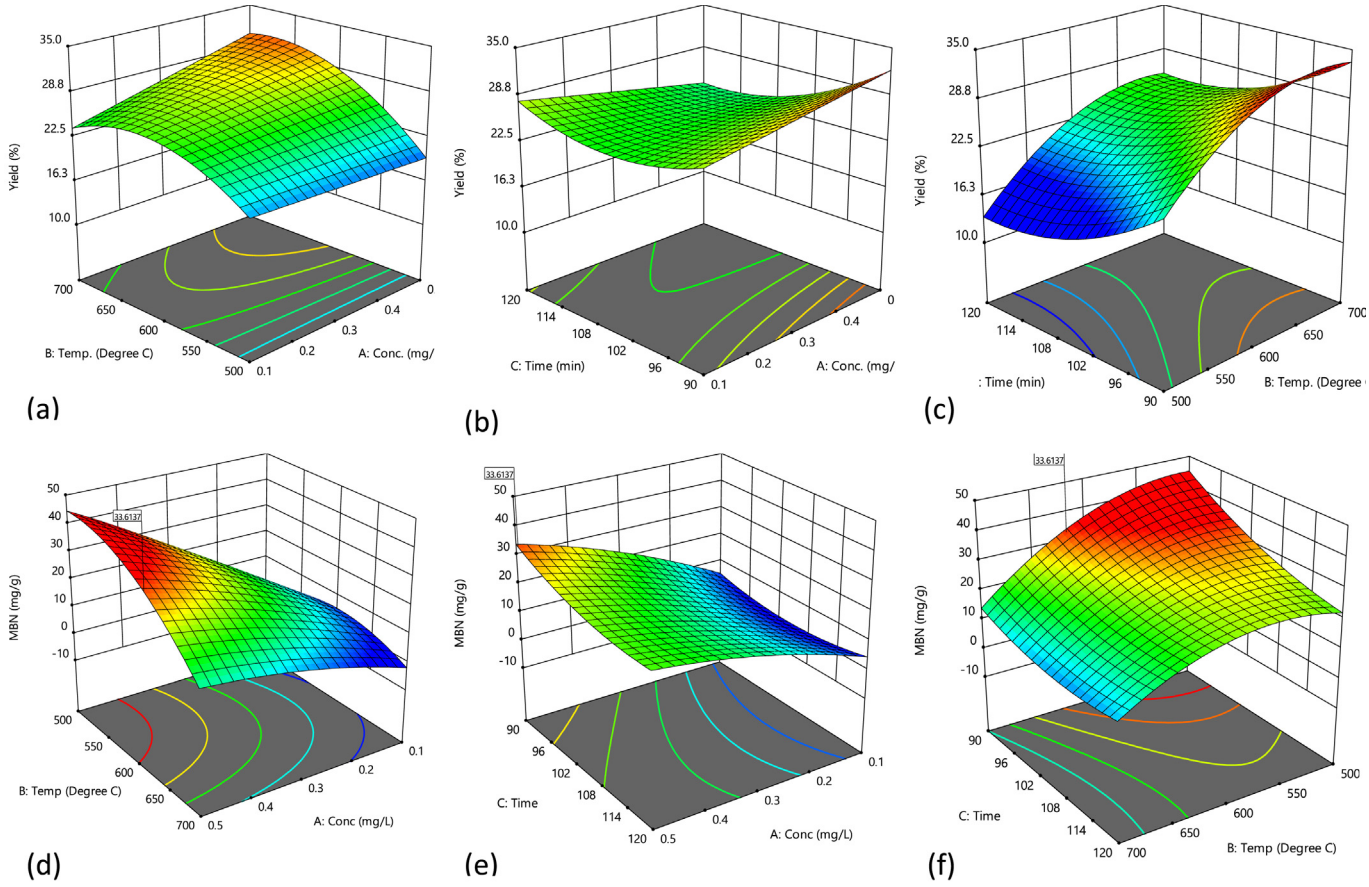

Figure 1. 3-D diagram showing effect of interaction of (a & d) Temperature and concentration (b & e) contact time and concentration (c & f) contact time and Temperature, on percentage yield and MBN of PKSAC.

different concentrations of phenol in a 100 ml conical flask that is covered with a glass stopper and subjected to various time (30–150 min) and agitation rate (150–250 rpm). A total of 29 flasks were used to carry out the experiments designed using statistics shown in Table 2. The flasks were then placed in a water bath shaker (Model HZ 300) at a constant temperature of 30 °C until the equilibrium point was reached. The exception was for the experiments carried out to test the effect of temperature.

2.6. Isotherm studies

Adsorption isotherms provide important information that describes the interaction of adsorbates with adsorbents. The amount of adsorbate attached to the surface of adsorbent is provided as a function of its concentration at a constant temperature. The graphical method was used and so the four popular isotherms (Langmuir, Freundlich, Temkin, and Dubinin-Radushkevich) were linearized into forms presented in order of Eqs. (4), (5), (6), and (7).

$$\frac{C_e}{q_e} = \frac{1}{k_l q_m} + c_e \frac{1}{q_m} \tag{4}$$

$$\ln q_e = \frac{1}{n} \ln c_e + \ln k_f \tag{5}$$

$$q_e = B \ln A + B \ln c_e \tag{6}$$

$$\ln q_e = \ln q_m - \beta \in^2 \tag{7}$$

The Langmuir isotherm assumes that intermolecular forces between the molecules of the adsorbate decrease quickly with distance. It is applied in this study to examine the presence of monolayer coverage of the adsorbate on the outer surface of the adsorbent. The Freundlich isotherm on the other hand assumes that ions adsorption happens on a heterogeneous medium through multilayer means in such a way that the number of ions adsorbed increases infinitely with concentration. The model is used in this study to investigate the existence of heterogeneity on the surface of the activated carbon while adsorbing phenol. The Temkin isotherm assumes that the heat of adsorption of the molecules of the adsorbate decreases proportionately with adsorbent layer coverage due to adsorbate-adsorbent interactions. It was considered in this study to predict the adsorbent-adsorbate relationship and the heat energy used in the adsorption of phenol. The Dubinin-Radushkevich isotherm model was employed to examine the free energy, E, and the characteristics of the adsorption process.

Table 4. Comparison of yield and MBN of some AC produced using palm kernel shell.

	Process parameters			Response	
	Temperature (°C)	Time (min)	Concentration (mg/L)	Yield (%)	MBN (mg/g)
This study	608.9	90.02	KOH	32.3 ± 20**	35.3 ± 11**
Wan et al. (2001)	500–900	60	-	24–29	-
Abechi et al. (2013)	1000	45	KOH	19.25	
Rajeshwar (2016)	400	240	H_3PO_4	-	260
Ulfah et al. (2016)	500	30–60	-	47.67–48.82	14.3–21.6
Norulaina et al. (2017)	500	120	NaOH	18.5–43.6	-
Andas et al. (2017)	700	30	-	8.931	994.83
Rashidi and Yusup (2017)	850	60	CO_2	25.15	-
Omar et al. (2017)	829.4	85	KOH	-	41.2
Sensitivity 1	608.0	30	0.5	27.3 ± 15	33.7 ± 17
Sensitivity 2	608.0	60	0.5	34.1 ± 08	36.0 ± 05

** After laboratory validation.

Table 5. Surface characteristics, proximate contents, and elemental analyses of precursor, char, PKSAC and Ag-NPs-PKSAC.

Properties	Sample			
	PKS	Char	PKSAC	Ag-NPs-PKSAC
BET surface area (m^2/g)	-	248.130	363.423	298.220
Total pore volume (cm^3/g)	-	0.087	0.169	0.137
Micropore volume (cm^3/g)	-	0.121	0.146	0.120
Porosity (%)		21	58	62
Average pore diameter (Å)	-	-	-	16.2
Proximate Analysis (%)				
Moisture content	7.3	6.6	5.9	5.7
Volatile matter	71.1	29.0	18.9	19.0
Fixed Carbon	18.5	59.7	69.2	69.3
Ash	3.1	4.7	6.0	6.0
Elemental Analysis (%)				
Carbon	49.2	63.7	76.3	76.3
Hydrogen	5.9	4.5	4.2	4.2
Nitrogen	0.6	0.5	0.5	0.5
Others	44.3	31.3	19.1	19.0

2.7. Kinetic studies

Analysis of kinetic data is needed to understand the adsorption mechanism and predict diffusion, and the kinetic transport that controls the adsorption rate. Because empirical models such as exponential, hyperbolic, logarithmic, and power models are difficult to associate with the given mechanisms of the adsorption process, models that have physical meaning are used in this study. The linearized form of pseudo-first-order, pseudo-second-order, and intra-particle diffusion models are presented in Eqs. (8), (9), and (10).

(1) Pseudo-first order

$$\log(q_e - q_t) = \log q_e - \left(\frac{k_1}{2.303}\right)t \tag{8}$$

(2) Pseudo-second order

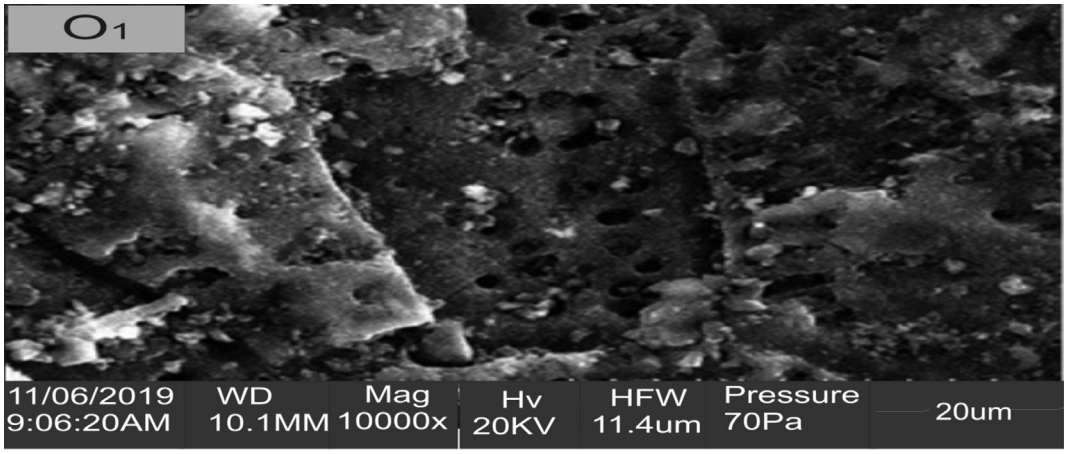

(a)

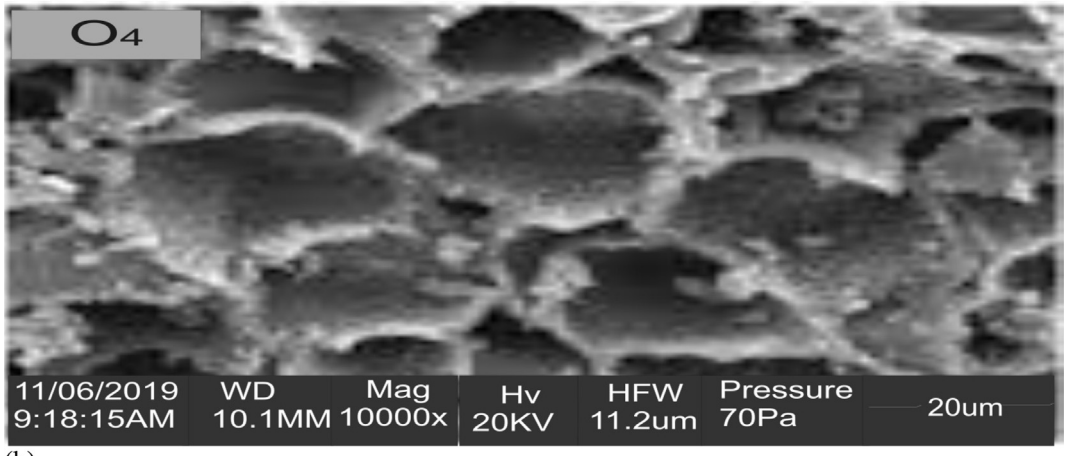

(b)

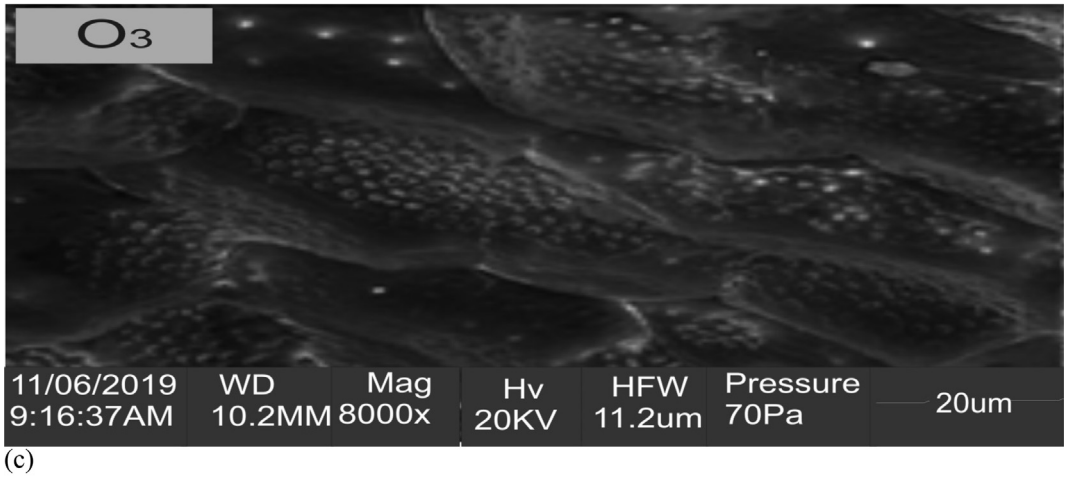

(c)

Figure 2. SEM images showing (a) raw PKS (b) PKSAC and (c) Ag-NPs-PKSAC.

$$\frac{t}{q_t} = \frac{1}{k_2 q_e^2} + \left(\frac{1}{q_e}\right) t \quad (9)$$

(3) Intra-particle diffusion model

$$q_t = k_{id} t^{0.5} + c \quad (10)$$

The graphical analysis of pseudo-first-order kinetics involves making plots of ln (q_e–q_t) versus t. the graph would be a straight line with a negative slope of k_1 and intercept of ln q_e. For the pseudo-second-order model, the plot of t/q_t versus t will produce a straight line with slope and intercept of $1/q_e$ and $1/k_2 q_e^2$, respectively. The selection of the appropriate model was based on the correlation coefficient (R^2). The model that best describes the process is that with the highest R^2 value. For the intra-particle diffusion model, a graph of q_t against $t^{1/2}$ will give a straight line with the slope of k_{dif} and intercept of C. Intra-particle diffusion model was investigated to identify the dominant mechanism controlling adsorption kinetics.

2.8. Adsorption thermodynamics

The value of changes in standard enthalpy (ΔH°), Gibbs free energy (ΔG°) and standard entropy (ΔSo) was computed from the adsorption data obtained at different temperature using the following equation:

$$\Delta G^0 = -RT \ln K_C \quad (11)$$

$$\ln k_L = \frac{\Delta s}{R} - \frac{\Delta H}{R}\left(\frac{1}{T}\right) \quad (12)$$

Where, R is the universal gas constant (8.314 J/mol k), T = absolute temperature (K), k_L is the Langmuir equilibrium constant (L/mg).

3. Results and discussion

3.1. Multi-objective function optimization for synthesis of AC

From Table 1, PKSAC yields varied between 17.9 - 32.3% which is an indication of the effects of different levels of process parameters. MBN is an indicator of the adsorptive capacity of PKSAC and can provide a quick assessment of the quality of the AC. The maximum MBN recorded is 35.88 mgg^{-1} and corresponds to sample 14. The relationship between the responses and various process variables was approximated by quadratic models (Eqs. (13) and (14)). Table 3 shows the analysis of variance (ANOVA) which confirmed the predictability of quadratic models for the yield and MBN with F-value of 20.54 and 23.07, respectively. The p – values recorded were less than 0.05 which indicates the reliability of the analysis with a 95 percent confidence level.

$$Yield\ (\%) = 2.8499 + 20.3365*Conc + 0.4732*Temp - 2.4233*Time + 0.0981*Conc*Temp - 0.75583*Conc*Time - 0.00387*Temp^2 + 0.011983*Time^2 \quad (13)$$

$$MBN = 6.80881 + 441.04625*Conc + 0.760882*Temp - 5.17648*Time - 0.402875*Con*Temp - 0.904167*\text{Conc}*Time + 0.003018*\text{Temp}*\text{Time} - 62.74375*Conc^2 - 0.000821*Temp^2 + 0.016001*Time^2 \quad (14)$$

3.2. Effects of factors on yield and MBN

Figure 1 shows the 3D graph for the main factor and their interactions on the yield and MBN of AC produced. It is evident from Figure 1(c & f) that the temperature and residence time exhibit a significant effect on the yield and MBN values. At the minimum temperature (500 °C) and for 90 min of residence time, the value of yield and MBN are approximately 12% and 37 mgg^{-1}, respectively. As the residence time increases from 90 to 120 min, there was a disproportionate decrease in yield and MBN which could be attributed to the release of C and other elements including H and O (Daud et al., 2001). However, as temperature increased between 500 - 600 °C, yield and MBN significantly increased with higher values obtained at 90 min. It was however observed that with a further increase in temperature above 620 °C, the values of the AC yield and MBN decreased significantly. This occurrence could be attributed to the loss of more heteroatoms at temperatures above 600 °C which got worse as residence time extended beyond 90 min in the furnace. This consequently reduced the char yield and adsorptive capacity indicated by reduced MBN (Rodriguez-Reinoso et al., 1982). The magnitude of MBN obtained for all samples indicated the distribution of mesopore in the AC produced. The carbonization temperature had the most significant effect in the pore structure of AC and therefore the adsorption capacity. The highest value of MBN was obtained around 610 °C where some micropores became widened when more volatile matters had escaped (Rajeshwar, 2016). Figure 1(e) shows the interaction of activation concentration and residence time. MBN of PKSACs increases with the concentration of KOH. The highest value was obtained at 90 min which decreases as residence time approaches 120 min. A similar trend was observed for the yield. The reduction of MBN and yield may be a result of the degeneration of pores caused by the prolonged activity of concentrated alkali during carbonization.

Eqs. (11) and (12) represent objective functions in numerical optimization. Yield and MBN were maximized subject to temperature (500–700 °C), residence time (90–120 min), and KOH concentration (0.1–0.5 M). The maximum yield and MBN of 32.3% and 36.28 mgg^{-1} were obtained at 608.8 °C, 90 min, and 0.495 M KOH (desirability = 0.99). The validity of numerical values was established experimentally, and the value of 33.9 ± 0.3 percent and 36.9 ± 0.02 mgg^{-1} for yield and MBN confirmed the consistency and representativeness of the models for prediction purposes.

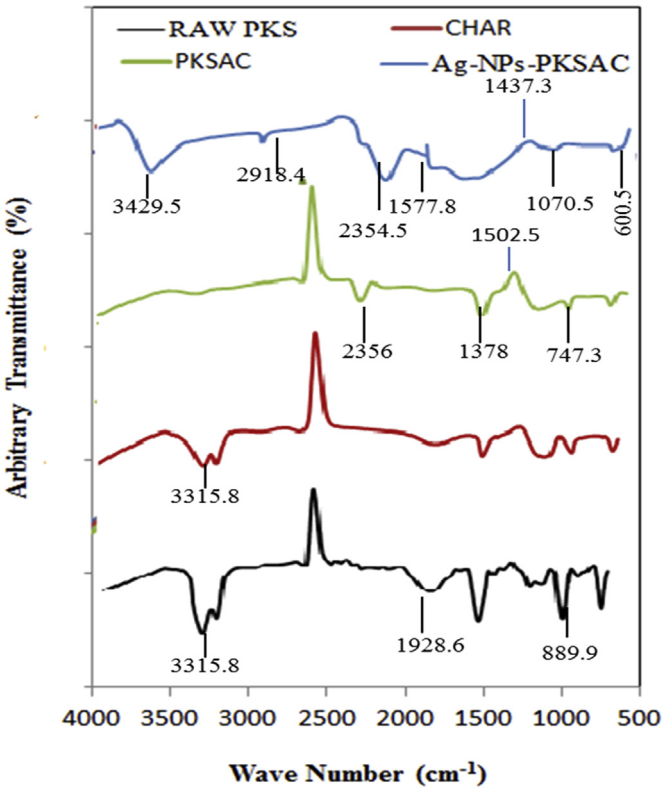

Figure 3. FTIR spectra of raw PKS, Char, PKSAC and Ag-NPs-PKSAC samples.

The sensitivity study for the effect of carbonization time on MBN and yield of the PKSACs was investigated by varying the time between 30 – 90 min while other parameters were kept constant at 608 °C and 0.5M KOH. A significant yield increase with the time between 30 - 60 min was observed. MBN, however, showed a marginal increment which may be attributed to the widening of micropores and consequent formation of mesopores. The synthesis of PKSAC was therefore achieved at 608 °C, 0.5 mol/dm^3 KOH (AC: KOH = 1), and carbonization holding time of 60 min. Table 4 shows how the yield and MBN obtained in this present study compared with some reported results from previous studies.

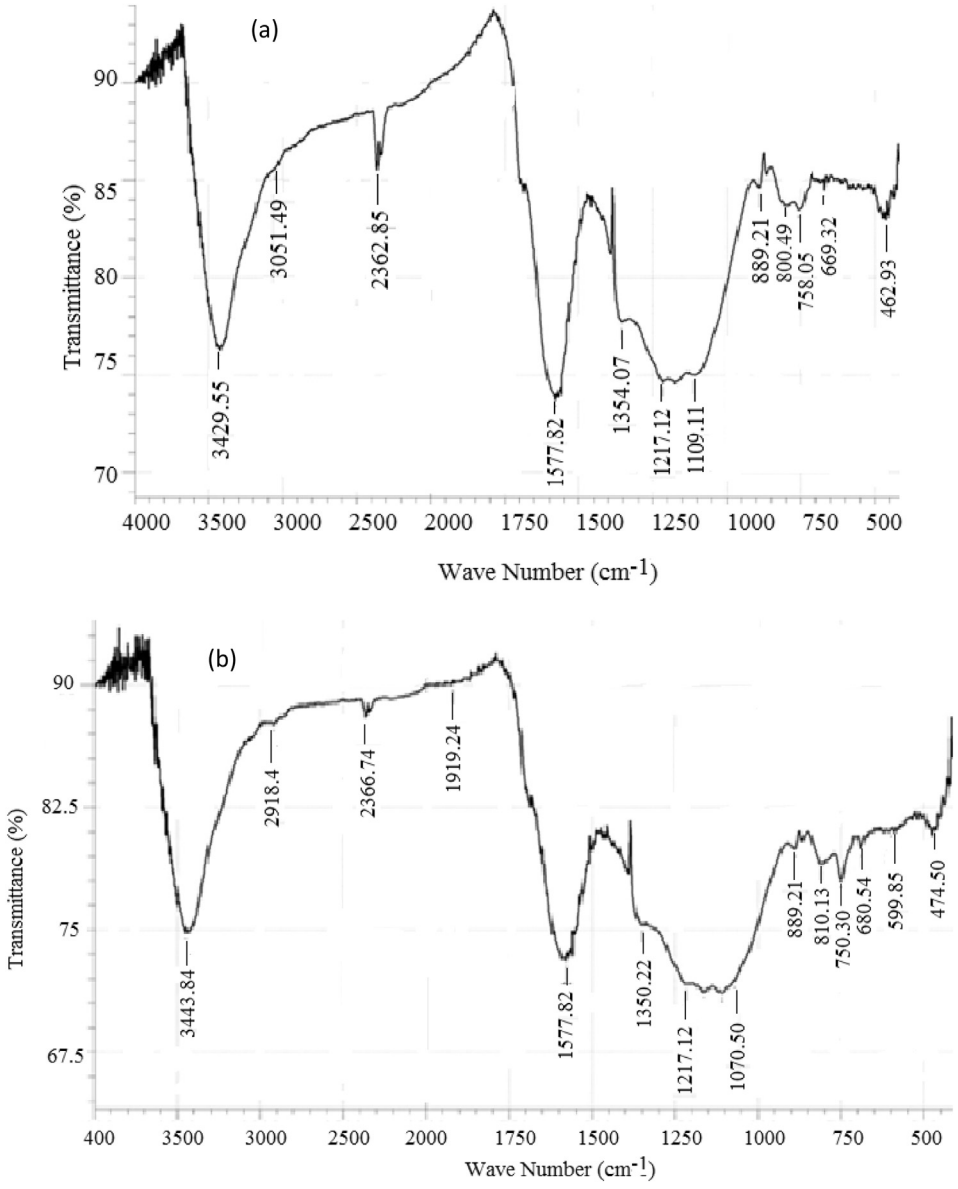

Figure 4. FTIR spectra of (a) wastewater and (b) treated water.

Table 6. Characteristics of wastewater and treated wastewater FTIR Spectra.

Frequency (cm^{-1})		Differences	Assignments
Wastewater	Treated Wastewater		
3449.55	3443.84	+5.71	O–H Stretching of hydroxyl group
3051.49	2918.4	+133.09	Aliphatic C–H group
2373.85	2366.74	+7.11	C–H stretching
1354.07	1350.32	+3.75	C–H bonding in alkanes
1109.11	1070.5	+38.61	–CO stretching in ester, ether group
810.49	810.13	+0.36	C–H out-of-plane bending in Benzene derivatives.
758.05	750.3	+7.75	C–H out of plane bending vibration
685.09	680.54	+4.55	C–Br stretch of alkyl halides
462.93	474.5	-11.57	–C bending functional groups

3.3. Characterization of ACs

Table 5 shows the proximate and ultimate analyses result for PKS, char, PKSAC, and Ag-NPs-PKSAC. A significant improvement of proximate properties of PKSAC when compared with the char and raw palm kernel shell was observed. Similar observations have been made for PKS and other agricultural residues processed for AC (Andas et al., 2017). Low volatile matter content increases char yield while low inorganic content such as ash is responsible for high fixed carbon content observed in Ag-NPs-PKSAC and PKSAC (Shamsuddina et al., 2016). The ultimate analysis showed that Ag-NPs-PKSAC and PKSAC have 76.3% of carbon which could be attributed to high organic content in PKS with huge potential for significant AC yield than most other sources (Jin et al., 2012; Koay et al., 2014).

The BET surface area obtained for PKSAC (363.4 m^2/g) is higher than that of Ag-NPs-PKSAC (363.423 n^2/g). The two products exhibited improved surface area than their char counterpart. However, Ag-NPs-PKSAC has better porosity (0.62 fractions) when compared with the others which imply better adsorbent. The 18% reduction of surface area in Ag-NPs-PKSAC compared to PKSAC was attributed to the modification with Ag nanoparticles (Ag-NPs) and implies that Ag-NPs had accumulated in micropores. In line with the IUPAC nomenclature, the different pores in porous materials can be described based on average diameters as micropores ($d < 20$ Å), mesopores ($20 < d < 500$ Å), and macropores ($d > 500$ Å). The average pore diameter estimated for Ag-NPs-PKSAC was 16.20 Å which falls in the micropores region and suggests that the adsorption of phenol could be occur more within the micropores. Also, it is evident from Table 5 that the micropores contributed heavily to the total available pores that characterized Ag-NPs-PKSAC. Approximately 87.6% of the total pores fall in the micro-scale region which suggests that the phenol entrapment at the surface of the AC would more likely be within the micropores spaces on the AC.

3.4. Surface morphology

SEM micrographs of raw PKS, PKSAC, and Ag-NPs-PKSAC produced are displayed in Figure 2(a), (b) and (c), respectively. The surface morphology of raw PKS (Figure 2a) showed intercalated and densely packed particles of low porosities. However, a significant pore structure with a series of rough cavities was observed in PKSAC as a result of the activation of the adsorbent using KOH. The phenomenon that led to the development of porosity was attributed to the thermal degradation of lignocellulosic material and the escape of volatile compounds (Ojedokun and Bello, 2017). These pores rendered a good surface for the phenol adsorption onto the surface of the PKSAC (Amin, 2008). Thus, activation at 608 °C with KOH resulted in the creation of more pores and the elimination of a large quantity of volatile matter. The modification of PKSAC by impregnation in Ag-NPs, resulted in a significant reduction in micropore volume due to Ag nanoparticles accumulation in micropores resulting in reductions of BET surface area and total pore volume. But there was an increase in pore diameter as evident in Figure 2(c). Large pore diameter observed in Ag-NPs-PKSAC is necessary for effective and efficient accommodation of phenol inside the pore spaces (Seredych et al., 2012).

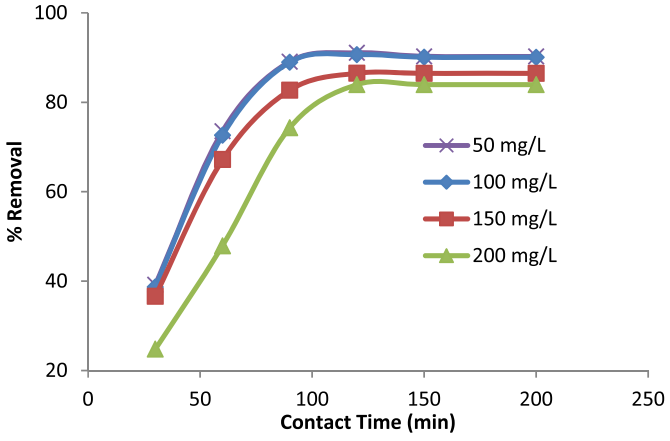

Figure 5. Percentage phenol removal as a function of contact time for various initial concentrations (dosage: 0.2 g, Agitation: 200 rpm).

3.5. Surface chemistry analysis

Fourier Transform Infrared Spectroscopy (FTIR) analysis performed indicates the prevalence of several functional groups on the adsorbents. Figure 3 presents an overlay of the FTIR spectra identified for raw PKS, char, PKSAC, and Ag-NPs-PKSAC. It is obvious some peaks had shifted, disappeared and some new peaks appeared due to carbonization, activation, and modification. It is also obvious from PKSAC spectra that the peaks were shifted marginally when compared with the char spectra. These shifts and disappearance in peaks are attributed to the influence of KOH used for activation. The FTIR spectroscopic analysis showed a wide band at 3429.5 cm^{-1} that appeared in Ag-NPs-PKSAC which signifies the O–H stretching of alcohol. The appearance of a peak observed at 2918.4 cm^{-1} in Ag-NPs-PKSAC spectra was due to the stretching vibration of C–H which emerged after the modification of PKSAC with Ag-nanoparticles. These newly emerged peaks are perhaps responsible for the improved adsorption performance of phenol observed in Ag-NPs-PKSAC over its PKSAC counterpart. The bands at 2354.5 and 2356 cm^{-1} are ascribed to the stretching of aldehydes. The double stretching vibration found in the aromatic ring occurs in PKSAC and Ag-NPs-PKSAC

Table 7. Experimental response for phenol adsorption onto Ag-NPs-PKSAC

Run	Factors				Response % Removal
	A:Agitation (rpm)	B:Time (min)	C:Dosage (g)	D:IConc (mg/L)	
1	0	0	0	0	87.31
2	0	1	1	0	89.27
3	-1	0	1	0	87.73
4	0	0	0	0	87.31
5	0	1	-1	0	88.08
6	0	0	-1	-1	81.00
7	0	-1	0	1	91.52
8	0	-1	-1	0	87.20
9	0	0	0	0	87.04
10	-1	0	0	-1	81.44
11	0	1	0	-1	81.92
12	0	1	0	1	91.16
13	-1	-1	0	0	87.89
14	1	1	0	0	87.57
15	0	0	0	0	86.99
16	1	0	0	1	89.96
17	1	0	-1	0	87.48
18	1	0	0	-1	80.72
19	0	0	1	-1	81.80
20	-1	1	0	0	87.47
21	1	0	1	0	87.00
22	1	-1	0	0	87.57
23	0	-1	1	0	89.13
24	-1	0	0	1	90.16
25	-1	0	-1	0	87.84
26	0	0	-1	1	90.00
27	0	0	1	1	90.65
28	0	-1	0	-1	82.96
29	0	0	0	0	87.09

corresponds to bands between 1502.5 and 1437.3 cm^{-1}. Both PKSAC and Ag-NPs-PKSAC have a peak at 1070.3 cm^{-1} due to presence of carbonyl group which confirmed the presence of the lignin structure (Garg et al., 2008).

Figure 4 however, shows the different peaks observed between the wastewater and treated water after adsorption using Ag-NPs-PKSAC sample. Table 6 shows the functional group present in wastewater and treated water. The differences in frequencies indicated that phenol pollutants have been deposited on the surface of the adsorbent.

4. Batch adsorption studies

Two sets of experiments were conducted to study the adsorption of phenol on Ag-NPs-PKSAC adsorbent. A set of experiments were performed to study the effects of the initial concentration of phenol and contact time on phenol uptake by Ag-NPs-PKSAC adsorbent. This was achieved by varying the initial concentration (50–200 mg/L) and contact time (30–200 min) while fixing the adsorbent dosage and agitation at 0.2 g and 200 rpm, respectively.

Another set of experiments was carried out using Box-Behnken design to determine the optimal process parameters that maximize the uptake of phenol by Ag-NPs-PKSAC adsorbent. Here, the factors selected include initial phenol concentration, contact time, adsorbent dosage, and agitation rate (Table 2).

4.1. Influence of initial phenol concentration and contact time

Figure 5 shows the characteristics of % phenol removal for various contact time and initial phenol concentration (50–200 mg/L) at 30 °C. The phenol uptake by the adsorbent improved with time at the onset due to the presence of vacant sites on the Ag-NPs-PKAC. A strong driving force in excess of the mass transfer resistance between aqueous and solid phases was developed. This was responsible for speedy phenol molecules uptake at the beginning which later decreased before reaching equilibrium. At the equilibrium, the maximum phenol uptake was attained because the vacant sites on the adsorbent could not be loaded with phenol molecules due to the repulsive forces between the phenol molecules and the adsorbent surfaces (Bello et al., 2019). The initial phenol concentration influenced both the phenol removed and the equilibrium time. At 100 mg/L initial concentration, the maximum adsorption uptake was 90.06% while that at 200 mg/L was 83.95%. At lower phenol initial concentration (ratio of phenol molecules to vacant sites was smaller), the amount of phenol adsorbed at equilibrium was high because there was more vacant site on Ag-NPs-PKSAC. As the ratio increased by an increase in the initial phenol concentration, the vacant sites easily become saturated and phenol molecules tend to compete to diffuse into the internal pores, resulting in lower percentage uptake on the surface of the adsorbent (Bello et al., 2019). From this experiment, there was no significant increase in %Removal after 2 h for all concentrations. Therefore, contact time (60–120 min) and concentration (100–200 mg/L) were selected for use in the Box-Behnken experiment.

5. Data analysis

Table 7 is the design matrix for the Box-Behnken method showing the 29 experimental runs performed for optimization. Table 8 shows the ANOVA table obtained after the data analysis. The F (1209.48) and p (<0.0001) values obtained at $\alpha = 0.05$, indicate a high level of confidence of using the developed quadratic model (Eq. (13)) to predict phenol adsorption from aqueous solution. The estimated regression coefficients for all linear process variables exhibit a significant effect with more than 99% confidence level ($p < 0.01$). However, the contact time being negative shows the adsorption becomes unfavorable if the contact time is prolonged more than necessary (Bello et al., 2019). The interactions of independent factors except the agitation-initial concentration are significant above 95% confidence level. The effect of the quadratic coefficient of agitation, contact time, and initial concentration were significant for the adsorption of phenol. However, the quadratic coefficient of agitation and initial concentration being negative implies a reduction of efficiency of adsorption as these parameters increase. As a separate model, the effect of main factors (F), the interactions of factors (2F), and quadratic effects were significant for phenol adsorption; they cannot individually approximate the adsorption of phenol due to the complexity of the process. Hence, the combination of main factors, factorial interaction and quadratic factors produced the needed synergy to produce a good proxy model for phenol adsorption from aqueous solution. The correlation coefficients ($R^2 = 0.9991$) and adjusted correlation coefficient (adj.$R^2 = 0.9983$) obtained are close to unity which indicates the suitability of the quadratic model for prediction and sampling experimental space for optimization purpose.

$$\begin{aligned}\%\ \text{removal} = {} & 51.5399 + 0.098\text{*Agitation} - 0.112\text{*Time} + 87.755\text{*Dosage} \\ & + 0.2054\text{*Iconc.} - 0.208\text{*Agitation*Dosage} + 0.00005\text{*Agitation*Iconc.} \\ & - 0.438\text{*Time*Dosage} + 0.00011\text{*Time*Iconc.} - 0.00017\text{Agitation}^2 \\ & + 0.0009\text{Time}^{\,2} - 0.00046\text{Iconc}^2\end{aligned} \tag{15}$$

Table 8. Analysis of Variance for phenol uptake by Ag-NPs-PKSAC.

Source	Sum of Squares	df	Mean Square	F-value	p-value	
Model	261.27	11	23.75	1209.48	<0.0001	significant
A-Agitation	0.2754	1	0.2754	14.03	0.0028	
B-Time	0.5776	1	0.5776	29.41	0.0002	
C-Dosage	0.6775	1	0.6775	34.50	<0.0001	
D-IConc	239.50	1	239.50	12195.70	<0.0001	
AC	0.1775	1	0.1775	9.04	0.0109	
AD	0.0676	1	0.0676	3.44	0.0883*	
BC	1.05	1	1.05	53.38	<0.0001	
BD	0.1156	1	0.1156	5.89	0.0320	
A^2	0.8728	1	0.8728	44.44	<0.0001	
B^2	3.79	1	3.79	192.81	<0.0001	
D^2	6.68	1	6.68	340.39	<0.0001	
Residual	0.2357	12	0.0196			
Lack of Fit	0.1432	8	0.0179	0.7741	0.6498	not significant
Pure Error	0.0925	4	0.0231			
Cor Total	261.51	23				

Table 9. Simulation and experimental values of phenol uptake from different adsorbents.

	Process variables				% phenol removal		
	Contact time (min)	IConc. (mg/L)	Agitation (rpm)	Dosage (g)	Ag-NPs-PKSAC	PKSAC	Synthetic
Simulattion	74.046	199.274	156.225	0.249	91.55	-	-
Experimental*	74	200	156	0.25	90.29 ± 0.73	85.64 ± 1.04	91.70 ± 0.02

* Average values with standard deviation.

Eq. (15) represents the objective function maximized subject to the constraints shown in Table 2. The maximum percentage phenol removal of 91.55% (Desirability = 1) was obtained after numerical optimization under the following operating conditions: Agitation rate (156.225 rpm), contact time (74.046 min), adsorbent dosage (0.249 g) and initial phenol concentration (199.274 mg/L). Table 9 shows the validated experiments performed in triplicates at the optimum process condition. The efficiency of the modified adsorbent was also compared with PKSAC and Synthetic adsorbents. The closeness of simulated and experimental values for Ag-NPs-PKSAC pointed to the reliability of the developed equation for predicting percentage phenol removal. Also, the modification of PKSAC using Ag-nanoparticles shows remarkable improvement over PKSAC, the result which competes very well with the commercial sample.

6. Adsorption isotherm

The experimental data generated at optimum conditions for different initial phenol concentrations (50–250 mg/L) were fitted to Langmuir, Freundlich, Temkin, and DB-R isotherms using the regression technique. The correlation coefficient (R^2) and adsorption capacity (Q_m) obtained were used as criteria for selecting a suitable model. Figure 6 shows the 2D-plot of the linearized form of four isotherm models evaluated in this study with the coefficient of correlation ranging between 0.876 – 0.9968. The model with R^2 closest to unity is considered superior using this criterion. This corresponds to the Langmuir isotherm (R^2 = 99.68%). The detail of the parameters estimated for various isotherms is tabulated in Table 10. Langmuir isotherm assumes monolayer adsorption, the maximum of which occurs when the surface is covered by a monolayer of adsorbate (Ogunleye et al., 2020). The optimum capacity of adsorbent can, therefore, be determined using the Langmuir model. As shown in Table 10, the maximum adsorption capacity (Q_{max}) of Ag-NPs-PKSAC for phenol uptake was 28.33 mgg^{-1}. The parameter R_L determines the shape of the isotherm. The process is favourable if $0 < R_L < 1$. It is irreversible if $R_L = 0$, linear if $R_L = 1$ and irreversible or unfavorable if $R_L > 1$ (Girish and Ramachandra, 2014). The value of R_L (0.082) obtained show favorable adsorption. Freundlich isotherm reveals non-ideal heterogeneous behaviour of the adsorption process (Bello et al., 2019). The value of parameter K_F of 2.138 indicates a relatively slow adsorption process. The value of n estimated was greater than 1. The Temkin model indicates the energy distribution pattern in the adsorbent layers. The equilibrium binding constant, B of 6.16 mol/g was determined from the Temkin isotherm graph. The porosity, free energy, E, and adoption mechanism are determined from the

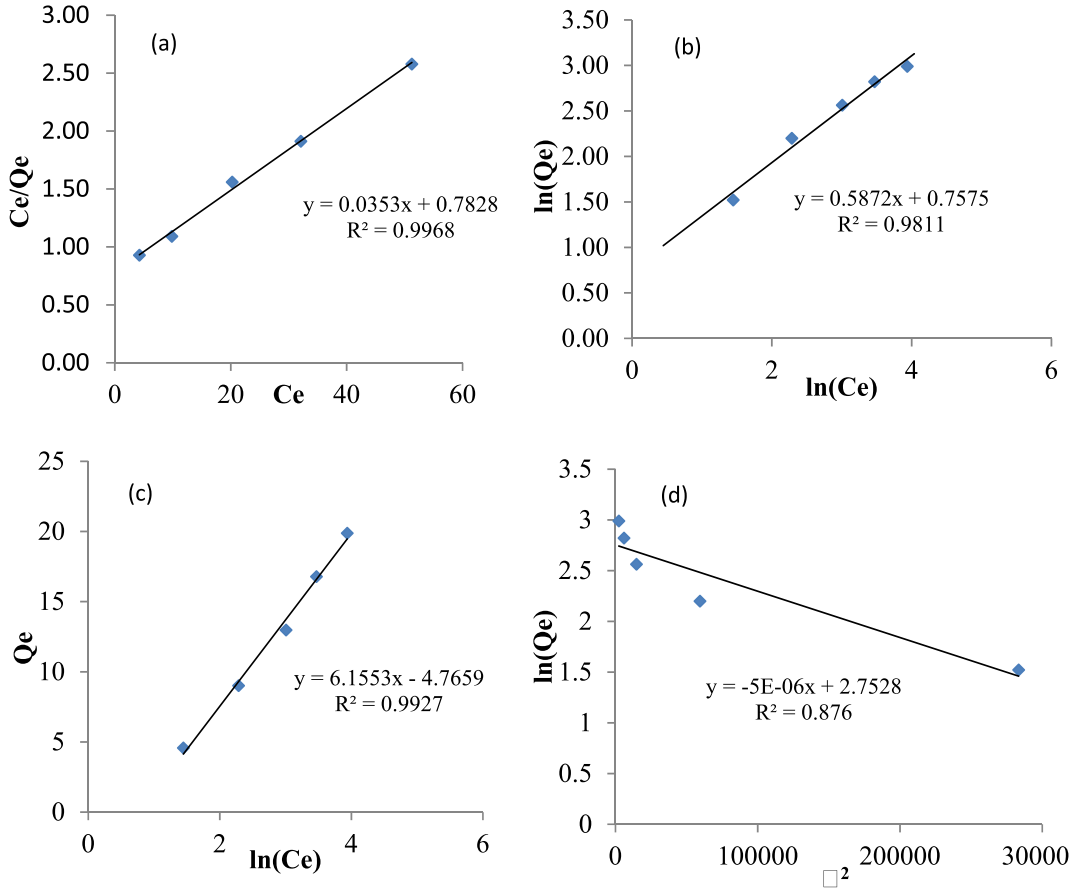

Figure 6. Plots of: (a) Langmuir, (b) Freundlich, (c) Temkin, (d) DB-R isotherms for phenol adsorption at 303 K.

Table 10. Parameter of isotherm models for phenol adsorption.

Isotherm	Linearization	plot	parameter	value
Langmuir	$\frac{C_e}{q_e} = \frac{1}{k_l q_m} + c_e \frac{1}{q_m}$	$\frac{C_e}{q_e}$ Vs c_e	Q_{max} (mgg^{-1})	28.33
			K_L (Lmg^{-1})	0.0513
			R_L	0.082
			R^2	0.997
Freundlich	$\ln q_e = \frac{1}{n} \ln c_e + \ln k_f$	$\ln q_e$ Vs $\ln c_e$	KF (mgg^{-1})	2.138
			n	1.695
			R^2	0.981
Temkin	$q_e = B \ln A + B \ln c_e$	q_e Vsln c_e	B	6.16
			A	0.461
			R^2	0.993
Dubnin-Radushkevich	$\ln q_e = \ln q_m - \beta \in^2$	$\ln q_e$ Vs $\in^2$	Q_{max} (mgg^{-1})	15.64
			$\beta(mg^2KJ^{-1})*10^{-4}$	0.05
			E (KJmol)	3.16
			R^2	0.876

Dubinin-Radushkevich isotherm plot. The E value of 3.16 $KJmol^{-1}$ obtained lies between 1 - 8 $KJmol^{-1}$ (Bello et al., 2019) which indicates physical adsorption. Based on this analysis, the adsorption of phenol on the surface of Ag-NPs-PKSAC is best described using the Langmuir model.

7. Adsorption kinetics

The kinetics of adsorption provides information (optimum volume) needed for sorption reactor design. The equilibrium data obtained were fitted with pseudo-first-order, pseudo-second-order, and intra-particle diffusion models. Table 11 shows various calculated parameters after fitting the experimental data. By using the correlation coefficient (R-square values) criteria, it was observed that the adsorption of phenol on the Ag-NPs-PKSAC obeys the pseudo-second-order kinetics with R-square value ranged between 0.94 – 0.96. Figure 7 shows the plot of Pseudo-second order kinetic for phenol adsorption onto Ag-NPs-PKSAC at 303K.

8. Adsorption thermodynamics

Adsorption thermodynamic provides information about the effect of temperature on the adsorption process. This was achieved by performing experiments at different temperatures (303–323 K) for various initial phenol concentrations (50–200 mg/L). When the graph of $\ln K_L$ *vs* $^1/_T$ *is* plotted as shown in Figure 8, ΔH^o and ΔS^o were

Table 11. Kinetic parameters for phenol adsorption.

Co (mg/L)	Q_e, exp. (mgg^{-1})	Pseudo-first order			Pseudo-second order			Intra-particle diffusion	
		$Q_{e,cal}$ (mgg^{-1})	K_1 (min^{-1})	R^2	$Q_{e,cal}$ (mgg^{-1})	K_2 (min^{-1})	R^2	Kp ($mgg^{-1}min^{-0,5}$)	R^2
100	10.3	3.8	0.05	0.97	14.64	0.003	0.99	1.02	0.96
150	19.7	3.3	0.01	0.90	19.08	0.002	0.99	1.20	0.94
200	29.1	4.0	0.01	0.95	29.33	0.001	0.99	2.04	0.96

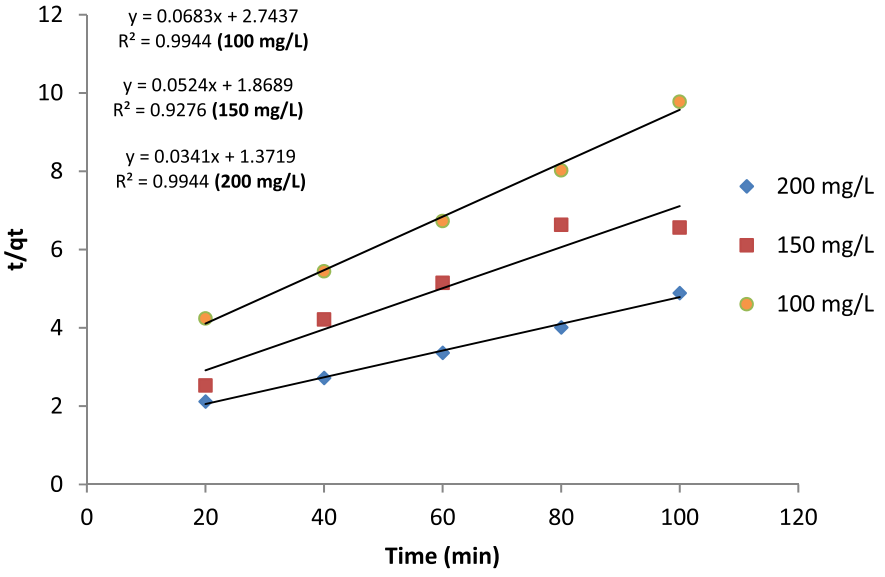

Figure 7. Plot of Pseudo-second order kinetic for phenol adsorption onto Ag-NPs-PKSAC at 303K.

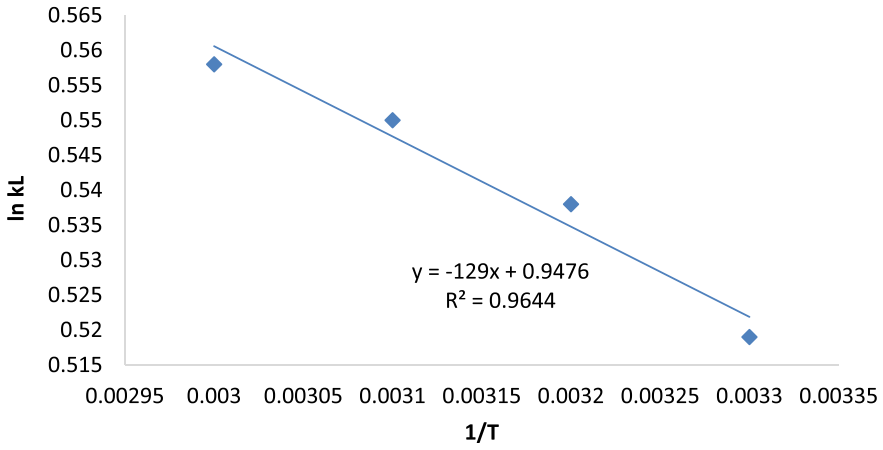

Figure 8. Plot of ln k_L against $\frac{1}{T}$.

Table 12. Thermodynamic parameters for adsorption of phenol.

ΔH^o (KJ/mol)	ΔS^o (KJ/molK)	ΔG^o (KJ/mol)		
		303 K	313 K	323 K
1.072	0.0079	-1.315	-1.472	-1.551

Table 13. Comparison of phenol %Removal efficiency of Ag-NPs-PKSAC with other green mediated AC.

Adsorbent	Phenol Removed	References
Coffee Residue	68.0%	Khenniche and Benissad-Aissani (2010)
Tea Industry waste	83.0%	Gundogdu et al. (2012)
Olive mill waste	85.0%	Abdelkreem (2013)
Luffa cylindrica fibers	65.5%	Abdelwahab and Amin (2013)
Olive stone	91.0%	Bohli et al. (2013)
Rice husk AC	95.0%	Ashanendu et al. (2019)
Rice husk AC	97.8%	Asgharnia et al. (2018)
Magnetic palm kernel biochar	93.4%	Hairuddin et al. (2019)
Palm kernel shell AC	85.6%	This study
Modified Palm kernel shell AC	90.3%	This study

estimated from the slope and intercept. The free energy (ΔG^o) was calculated using Eq. (11). Table 12 shows the thermodynamic parameters estimated for adsorption of phenol from aqueous solution using Ag-NPs-PKSAC. The positive nature of ΔH° means endothermic adsorption and therefore a temperature increase leads to an increase in the rate of diffusion of phenol molecules across the boundary layer and to the internal pores of the adsorbent particle (Wang and Zhu, 2007). The positive value of ΔS° indicates the degree of Ag-NPs-PKSAC affinity for phenol and also shows increasing randomness at the solid-solution interface during the adsorption process. The parameter ΔG° was negative so the process is feasible and spontaneous. It was therefore observed that the phenol adsorption on Ag-NPs-PKSAC was more favorable at the highest temperature (323K) due to the endothermic nature of the system. Table 13 shows the result of a comparative study of %removal obtained from this study with other known adsorbents. It is observed that the result of this study compared well with some well-known activated carbons that have been applied for phenol removal from aqueous solutions.

9. Conclusion

PKSAC was synthesized by optimization of MBN and yield criteria through a Box-Behnken experiment considering the effects of temperature, time, and KOH concentration. These criteria offer a simple and quick alternative characterization approach to sophisticated analytical equipment. Highly porous PKSAC with optimum MBN and Yield of 32.3 ± 20 mgg^{-1} and 35.3 ± 11% were successfully synthesized from PKS. The efficacy of PKSAC was improved by surface modification with Ag-nanoparticles. SEM analysis revealed a larger pore diameter in Ag-NPs-PKSAC compared to PKSAC and PKS. The increased pore diameter is desirable for effective and efficient accommodation of phenol inside the pore spaces. The %removal of phenol by PKSAC, Ag-NPs-PKSAC, and a commercial AC considering initial phenol concentration of 200 mg/L, 0.25 g adsorbent dosage, 74 min contact time, and 156 rpm agitation rate were 85.6, 90.3 and 91.7%, respectively. A quadratic-based predictive model of %removal against initial phenol concentration, adsorbent dosage, contact time, and the agitation rate was developed. The F and p statistics ($\alpha = 0.05$) show a significant correlation with coefficient and adjusted coefficients of 0.999 and 0.998. The kinetic studies indicated phenol adsorption onto Ag-NPs-PKSAC followed pseudo-second-order. The equilibrium data fit very well with the Langmuir isotherm with a physical adsorption mechanism.

The thermodynamic results showed the adsorption was spontaneous and endothermic, therefore; temperature increase results in the increased rate of phenol molecules diffusion across the boundary layer and to the internal pores of the adsorbent particle.

Declarations

Author contribution statement

Aremu, M.O.: Conceived and designed the experiments; Wrote the paper.

Arinkoola, A.O.: Conceived and designed the experiments; Analyzed and interpreted the data; Wrote the paper.

Olowonyo, I.A: Performed the experiments; Contributed reagents, materials, analysis tools or data.

Salam, K.K: Analyzed and interpreted the data; Wrote the paper.

Funding statement

This research did not receive any specific grant from funding agencies in the public, commercial, or not-for-profit sectors.

Competing interest statement

The authors declare no conflict of interest.

Additional information

No additional information is available for this paper.

Acknowledgements

The authors acknowledge Chemical Engineering and Material Science laboratories of both LAUTECH and African University of Science and Technology, (AUST), Abuja for characterization and technical support.

References

Abdelkreem, M., 2013. Adsorption of phenol from industrial wastewater using olive mill waste. APCBEE Proc. 5, 349–357.

Abdelwahab, O., Amin, N.K., 2013. Adsorption of phenol from aqueous solutions by Luffa cylindrica fibers: kinetics, isotherm and thermodynamic studies. Egypt J. Aquat. Res. 39, 215–223.

AbdelWahab, O., Amin, N.K., El-Ashtoukly, E.Z., 2009. Electrochemical removal of phenol from oil refinery wastewater. J. Hazard Mater. 163, 711–716.

Abechi, S.E., Gimba, C.E., A. U., Dallatu, Y.A., 2013. Preparation and characterization of activated carbon from palm kernel shell by chemical activation. Res. J. Chem. Sci. 3 (7), 54–61.

Amin, N.K., 2008. Removal of direct blue-106 dye from aqueous solution using new activated carbons developed from pomegranate peel: adsorption equilibrium and kinetics. J. Hazard Mater. 165, 52–62.

Andas, J., Rahman, M.L.A., Yahya, M.S.M., 2017. Preparation and characterization of activated carbon from palm kernel shell. Mater. Sci. Eng. 226, 012156, 2017.

Asgharnia, H., Nasehinia, H., Rostami, R., Rahmani, M., Mehdinia, S.M., 2018. Phenol removal from aqueous solution using silica and activated carbon derived from rice husk. Water Pract. Technol. 14 (4), 897–907.

Ashanendu, M., Paramartha, M., Sudip, K.D., 2019. Efficiency analysis of rice husk as adsorbent for removal of phenol from wastewater. J. Environ. Anal. Toxicol. 9, 3, 2019.

Balakrishnan, M., Batra, V.S., 2011. Valorization of solid waste in sugar factories with possible applications in India: a review. J. Environ. Manag. 92, 2886–2891.

Bello, O.S., Adegoke, K.A., Fagbenro, S.O., luwaseun, Lameed, O.S., 2019. Functionalized coconut husks for rhodamine-B dye sequestration. Appl. Water Sci. 9, 189.

Bhatnagar, A., Vilar, V.J.P., Botelho, C.M.S., Boaventura, R.A.R., 2011. A review of the use of red Mud as adsorbent for the removal of toxic pollutants from water and wastewater. Environ. Technol. 32, 231–249.

Bhatnagar, A., Sillanpää, M., Witekkrowiak, A., 2015. Agricultural waste peels as versatile biomass for water purification - a review. Chem. Eng. J. 270, 244–271.

Bohli, T., Fiol, N., Villaescusa, I., Ouederni, A., 2013. Adsorption on activated carbon from olive stones: kinetics and equilibrium of phenol removal from aqueous solution. J. Chem. Eng. Process Technol. 4, 165.

Busca, G., Berardinelli, S., Resini, C., Arrighi, L., 2008. Technologies for the removal of phenol from fluid streams: a short review of recent developments. J. Hazard Mater. 160, 265–288.

Cerqueira, A.A., Costa Marques, M.R., 2012. Electrolytic treatment of wastewater in the oil industry. In: New Technologies in the Oil and Gas Industry, INTECH, pp. 3–28.

Chebli, D., Bouguettoucha, A., Mekhalef, T., Nacef, S., Amrane, A., 2015. Valorization of an Gricultural Waste, Stipa Tenassicima Fibers, by Biosorption of an Anionic Ao Dye, Congo Red.

Cheung, W.H., Lau, W.H., Leung, S.S.Y., Ip, S.Y.A.W.M., McKay, G., 2012. Characteristics of chemical modified activated carbons from bamboo scaffolding. Chin. J. Chem. Eng. 20 (3), 515–523, 2012.

Daud, W.M.A.W., Ali, W.S.W., Sulaiman, M.Z., 2001. Effect of carbonization temperature on the yield and porosity of char produced from palm shell. J. Chem. Technol. Biotechnol. 76, 1281–1285.

Devi, P., Saroha, A.K., 2016. Utilization of sludge based adsorbents for the removal of various pollutants: a review. Sci. Total Environ. 578, 16–33.

El-Nas, M.H., Al-Zuhair, S., Makhlouf, S., 2009. Batch degradation of phenol by *Pseudomonas putida* immobilized in polyvinyl alcohol (PVA) gel. J. Hazard Mater. 164, 720–725.

Fuf, Wang, Q., 2011. Removal of heavy metals from wastewater. Rev. J. Environ. Manag. 92 (3), 407–418.

Gámiz, B., Pignatello, J.J., Cox, L., Hermosín, M.C., Celis, R., 2016. Environmental fate of the fungicide metalaxyl in soil amended with composted olive-mill waste and its biochar: an enantioselective study. Sci. Total Environ. 541, 776–783.

Garg, U., Kaur, M.P., Jawa, G.K., Sudi, D., Garg, V.K., 2008. Removal of cadmium (II) from aqueous solutions by adsorption on agricultural waste biomass. J. Hazard Mater. 154, 1149–1157.

Girish, C.R., Ramachandra, V., 2014. Adsorption of phenol from aqueous solution using Lantana Camara, Forest waste: kinetics, isotherm, and thermodynamic studies. Int. Sch. Res. Not. 14, 1–16.

Gundogdu, A., Duran, C., Basri Senturk, H., Soylak, M., Ozdes, D., Serencam, H., Imamoglu, M., 2012. Adsorption of phenol from aqueous solution on a low-cost activated carbon produced from tea industry waste: equilibrium, kinetic, and thermodynamic study. J. Chem. Eng. Data 57, 2733–2743, 2012.

Hafshejani, L.D., Hooshmand, A., Naseri, A.A., Mohammadi, A.S., Abbasi, F., Bhatnagar, A., 2016. Removal of nitrate from aqueous solution by modified sugarcane bagasse biochar. Ecol. Eng. 95, 101–111.

Hairuddin, M.N., Mubarak, N.M., Khalid, M., et al., 2019. Magnetic palm kernel biochar potential route for phenol removal from wastewater. Environ. Sci. Pollut. Res. 26, 35183–35197, 2019.

Jin, X., Yu, Z., Wu, Y.U., 2012. Preparation of activated carbon from lignin obtained by straw pulping by Koh and K 2 Co 3 chemical activation. J. Cell. Chem. Technol. 46, 79–85.

Karri, R.R., Jayakumar, N.S., Sahu, J.N., 2017. Modelling of fluidized bed reactor by differential 946 evolution optimization for phenol removal using coconut shells based activated carbon. J. Mol. Liq. 231, 249–262.

Khenniche, L., Benissad-Aissani, F., 2010. Adsorptive removal of phenol by coffee residue activated carbon and commercial activated carbon: equilibrium, kinetics, and thermodynamics. J. Chem. Eng. Data 55, 4677–4686, 2010.

Koay, Y.S., Ahamad, I.S., Nourouzi, M.M., Abdullah, L.C., Shean, T., Choong, Y., 2014. Com. Development of novel low-cost quaternized adsorbent from palm oil agriculture waste for reactive dye removal. Bio Resour. 9 (1), 66–85, 9(1974).

Lateef, A., Azeez, M.A., Asafa, T.B., Yekeen, T.A., Akinboro, A., Oladipo, I.C., Ajetomobi, F.E., Gueguim-Kana, E.B., Beukes, L.S., 2016. Cola nitida-mediated biogenic synthesis of silver nanoparticles using seed and seed shell extracts and evaluation of antibacterial activities. Bio. Nano Sci. 10, 551–562.

Murniati, M.D.G.L., Budianta, W., Rivera, K.K.P., Arazo, R.O., 2017. Removal of sodium diclofenac from aqueous solution by adsorbents derived from cocoa pod husks. J. Environ. Chem. Eng.

Nayak, A.K., Pal, A., 2017. Green and efficient biosorptive removal of methylene blue by Abelmoschus esculentus seed: process optimization and multi-variate modeling. J. Environ. Manag. 200, 145–159.

Norulaina, A., Muhammad, A.A.Z., Mohd, J.K., 2017. Roles of impregnation ratio of K2CO3 and NaOH in chemical activation of palm kernel shell. J. Appl. Sci. Proc. Eng. 4 (2), 2017.

Ogunleye, O.O., Arinkoola, A.O., Eletta, O.A., Agbede, O.O., Osho, Y.A., Morakinyo, A.F., Hamed, J.O., 2020. Green corrosion inhibition and adsorption characteristics of *Luffa cylindrical* leaf extract on mild steel in hydrochloric acid environment. Heliyon 6, e03205.

Ojedokun, A.T., Bello, O.S., 2017. Kinetic modeling of liquid-phase Adsorption of Congo red dye using Guava leaf-based activated carbon. Appl. Water Sci. 7, 1965–1977.

Okeowo, I.O., Balogun, E.O., Ademola, A.J., Alade, A.O., Afolabi, T.J., Dada, E.O., Farombi, A.G., 2020. Adsorption of phenol from wastewater using microwave-assisted Ag–Au nanoparticle-modified mango seed shell-activated carbon. Int. J. Environ. Res.

Omar, A., Ramesh, K., Alic, Gomaa A.M., Rosli, M.Y., 2017. Application of response surface methodology for optimization of palm kernel shell activated carbon preparation factors for removal of H_2S from industrial wastewater. Jurnal Teknologi 79 (7), 1–10, 2017.

Peña, D., López-Piñeiro, A., Albarrán, Á., Rato-Nunes, J.M., Sánchez-Llerena, J., Becerra, D., Ramírez, M., 2016. De-oiled two-phase olive mill waste may reduce water contamination by metribuzin. Sci. Total Environ. 541, 638–645.

Portinho, R., Zanella, O., Féris, L.A., 2017. Grape stalk application for caffeine removal through dsorption. J. Environ. Manag. 202, 178–187.

Rajeshwar, M.S., 2016. Effect of preparation parameters on methylene blue number of activated carbons prepared from a locally available material. J. Inst. Eng. 12 (1), 169–174, 2016.

Rashidi, Nor Adilla, Yusup, Suzana, 2017. Potential of palm kernel shell as activated carbon precursors through single stage activation technique for carbon dioxide adsorption. J. Clean. Prod.

Rodriguez-Reinoso, F., Gonzalez, J.D.L., Berenger, C., 1982. Activated carbon from almonds shells-I. Preparation and characterization by nitrogen adsorption. Carbon 20 (6), 513–518.

Seredych, M., Wu, C.T., Brender, P., Ania, C.O., Vix-Guterl, C., Bandosz, T.J., 2012. Role of phosphorus in carbon matrix in desulphurization of diesel fuel using adsorption process. Fuel 92, 318–326.

Shamsuddina, M.S., Yusoffa, N.R.N., Sulaimana, M.A., 2016. Synthesis and characterization of activated carbon produced from kenaf core fiber using H_3PO_4 activation. Proc. Chem. 19, 558–565, 2016.

Shourian, M., Noghabi, K., Zahin, H., Baghen, J., Karaballaei, G., Mollaei, M., 2009. Efficient phenol degradation by a newly characterized *Pseudomonas species.* isolated from pharmaceutical wastewater. Desalination Water Treat. 246, 577–594.

Trivedi, N.S., Mandavgane, S.A., Kulkarn, B.D., 2016. Mustard plant ash: a source of micronutrient and an adsorbent for removal of 2,4-dichlorophenoxyacetic acid. Environ. Sci. Pollut. Res. 23 (20), 20087–20099.

Ulfah, M., Raharjo, S., Hastuti, P., Darmadji, P., 2016. The potential of palm kernel shell activated carbon as an adsorbent for β-carotene recovery from crude palm oil. Advances of Science and Technology for Society. AIP Conf. Proc. 1755, 130016-1–130016-5.

Wan, M.A., Wan, D., Wan, S., Wan, A., Mohd Zaki, S., 2001. Effect of carbonization temperature on the yield and porosity of char produced from palm shell. J. Chem. Technol. Biotechnol. 76, 1281–1285.

Wan Ngah, W.S., Hanafiah, M.A.K.M., 2008. Removal of heavy metal ions from wastewater by chemically modified plant wastes as adsorbents: a review. Bioresour. Technol. 99, 3935–3948.

Wang, S., Zhu, Z.H., 2007. Effects of acidic treatment of activated carbons on dye adsorption. Dyes Pigments 75, 306–314.

Wang, H., Chu, Y.X., Fang, C.R., 2017. Sorption of tetracycline on biochar derived from rice straw under different temperatures. PloS One 12 (8), 1–14.

Wang, Y., Zhao, L., Hou, J., Peng, H., Wu, J., Liu, Z., Guo, X., 2018. Kinetic, isotherm, and thermodynamic studies of the adsorption of dyes from aqueous solution by cellulose-based adsorbents. Water Sci. Technol. 77, 2699–2708.

Yin, Y.Y., Guo, X.T., Yang, C., Gao, L.M., Hu, Y.B., 2016. An efficient method for tylosin removal from an aqueous solution by goethite modified straw mass. RSC Adv. 98, 95425–95434.

Zhang, Y., Geißen, S., Gal, C., 2017. Carbamazepine and diclofenac: removal in wastewater treatment plants and occurrence in water bodies. Chemosphere 73, 1151–1161.